Copyright © 2008 American Scientific Publishers
All rights reserved
Printed in the United States of America

Journal of
Computational and Theoretical Nanoscience
Vol. 5, 1128–1137, 2008

Formalism Application of the Non-Equilibrium Green's Function for the Numerical Analysis of Carbon Nanotube FETs

Mahdi Pourfath* and Hans Kosina

Institute for Microelectronics, TU Wien, Gusshausstrasse 27-29/E360, 1040 Vienna, Austria

A deeper understanding of quantum effects in nano-electronic devices helps to improve the performance and to develop new device types. Carbon nanotube-based transistors have been studied in recent years as potential alternatives to CMOS devices. The performance of carbon nanotube field-effect transistors is studied using the non-equilibrium Green's function formalism. Electron–phonon interaction parameters, such as electron–phonon coupling strength and phonon energy, strongly depend on the chirality and the diameter of the carbon nanotube. Therefore, the steady-state and dynamic response of carbon nanotube based transistors are studied for a wide range of electron–phonon interaction parameters.

Keywords: Carbon Nanotubes, Field Effect Transistors, Non-Equilibrium Green's Functions, Device Simulation.

RESEARCH ARTICLE

1. INTRODUCTION

Tremendous advances have been achieved in semiconductor technology during the past decades. With continuing efforts to improve speed and functionality of integrated circuits, the requirement of higher integration densities forces device dimensions to shrinks to the scale of the wave length of electrons.

Exceptional electronic and mechanical properties together with nano-scale diameter make carbon nanotubes (CNTs) promising candidates for nano-scale transistors. Ballistic transport in short CNT based transistors at room temperature has been reported.[1] CNTs can be considered as a graphene sheet which has been wrapped into a tube. The way the sheet is wrapped is represented by a pair of indices (n, m) called the chiral vector. The integers n and m denote the number of basis vectors along two directions in the honeycomb crystal lattice of graphite. The CNT is called *zigzag*, if $m = 0$, *armchair*, if $n = m$, and *chiral* otherwise. CNTs with $n - m = 3$ are metals, otherwise they are semiconductors.[2] Semiconducting CNTs can be used as a channel for transistors,[3] whereas metallic CNTs can serve as interconnect wires.[4] In this work we consider transistors based on semiconducting zigzag CNTs. Depending on the work function difference between the metal contact and the CNT, carriers at the metal-CNT interface encounter different barrier heights (see Fig. 1). Fabrication of devices with positive (Schottky type)[5] and zero (Ohmic)[6] barrier heights for holes have been reported.

With the aid of numerical analysis one can get a deeper insight into device operation and investigate methods to improve the device performance. Calculations based on the non-equilibrium Green's function formalism (NEGF) of current through electronic devices was first described in a series of papers in the early 1970s.[7–10] The NEGF technique has widely been used to study quantum transport of electrons and holes in a variety of materials and devices, such as III–V resonant tunneling diodes,[11–19] electron waveguides,[20] Si tunneling diodes[21,22] ultra-scaled Si MOSFETs,[23–25] CNTs,[26–41] metal wires,[42,43] and organic molecules.[44–50] We employed the NEGF formalism to perform a comprehensive numerical study of CNT based transistors.

The outline of the paper is as follows. In Section 2, the NEGF formalism is briefly described. The implementation of this method for CNT based transistors is presented in Section 3. The electron–phonon interaction parameters of a CNT depend on the chiral vector, which implies that many different parameter values exist. In Section 4 the device response is studied for a wide range of electron–phonon interaction parameters. After a brief discussion in Section 5, conclusions are drawn in Section 6.

*Author to whom correspondence should be addressed.

1546-1955/2008/5/1128/010 doi:10.1166/jctn.2008.011

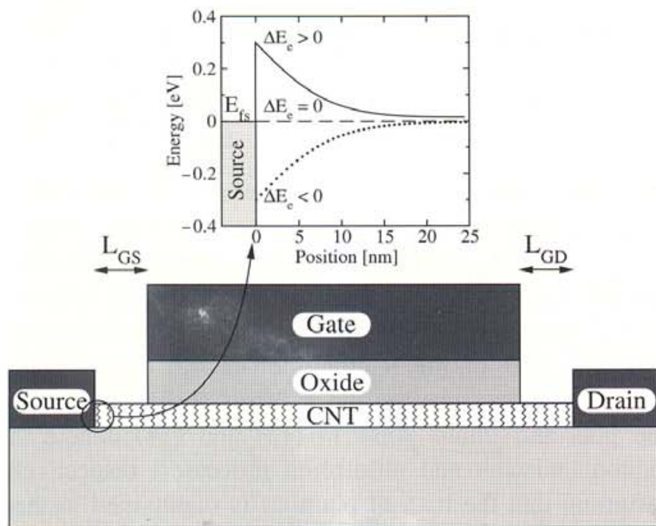

Fig. 1. Cross section of the investigated CNT based transistor and the band-edge profile at the source sided metal-CNT interface. Depending on the work function difference between metal and CNT, a positive, zero, or negative barrier height for electrons or holes can be achieved. In this work we assume electrons as majority carriers. Due to the symmetric band structure, the conclusions also hold for holes.

2. GOVERNING EQUATIONS

The NEGF technique initiated by Schwinger[51] and Kadanoff and Baym[52] allows one to study the time evolution of a many-particle quantum system. Knowing the single-particle Green's functions of a given system, one may evaluate single-particle quantities like carrier density or current. The many-particle information about the system is cast into self-energies, which are part of the equations of motion for the Green's functions. Perturbation expansion of the Green's functions is the key to approximate the self-energies. Green's functions provide a powerful technique to evaluate the properties of a many-body system both in thermodynamic equilibrium and non-equilibrium situations. Non-equilibrium conditions can be due to, e.g., an applied electric field, a light excitation pulse, or coupling to contacts at different electro chemical potentials.

2.1. The Non-Equilibrium Green's Function

The contour-ordered non-equilibrium Green's function is defined as

$$G(1,2) = -i\hbar^{-1}\langle T_C\{\hat{\psi}_H(1)\hat{\psi}_H^\dagger(2)\}\rangle \tag{1}$$

where the abbreviation $1 \equiv (\mathbf{r}_1, t_1)$ is used, $\hat{\psi}_H$ and $\hat{\psi}_H^\dagger$ are field operators in the Heisenberg picture, $\langle \ldots \rangle$ is the statistical average with respect to the density operator, and the contour ordering operator T_C orders the time labels according to their order on the contour C. The so defined Green's function satisfies the following equations of motion (Dyson equation)[53,54]

$$G(1,2) = G_0(1,2) + \int_C d3 \int_C d4 G_0(1,3)\Sigma(3,4)G(4,2) \tag{2}$$

where G_0 is the single-particle (non-interacting) Green's function, and the self-energy Σ describes the renormalization of G_0 due to the interaction with the surrounding many-particle system. The differential form of the Dyson equation is achieved by multiplying both sides of (2) by

$$G_0^{-1}(1,2) = [i\hbar\partial_{t_1} - H_0(1)]\delta(1-2) \tag{3}$$

where H_0 is the single-particle Hamiltonian. The general form of the single-particle Hamiltonian is given by

$$H_0(\mathbf{r},t) = -\frac{\hbar^2}{2m}\nabla_\mathbf{r} + U(\mathbf{r},t) \tag{4}$$

where the potential energy U includes the effects of the Crystal potential and the Hartree potential which is in fact the solution of the Poisson equation.

The contour representation is rather impractical for calculations, and one prefers to work with real time integrals. The different forms of non-equilibrium theory employ different methods for converting the contour into usual time integration. Neglecting initial correlations,[53] Keldysh introduced the contour C_K which consists of two parts:[55] C_1 extending from $-\infty$ to ∞ and C_2 extending from ∞ to $-\infty$. Each of the time arguments t_1 and t_2 in (1) can reside either on the first or the second part of the contour. Therefore, the contour-ordered Green's function contains four functions G_t (time-ordered), $G_{\bar{t}}$ (anti time-ordered), $G^>$ (greater), and $G^<$ (lesser), which are defined as[55]

$$G(1,2) = \begin{cases} G_t(1,2) & t_1, t_2 \in C_1 \\ G_{\bar{t}}(1,2) & t_1, t_2 \in C_2 \\ G^>(1,2) & t_1 \in C_2, t_2 \in C_1 \\ G^<(1,2) & t_1 \in C_1, t_2 \in C_2 \end{cases} \tag{5}$$

Since $G_t + G_{\bar{t}} = G^< + G^>$, there are only three linearly independent functions, reflecting a freedom of choice. For our purpose the most suitable Green's functions are the $G^\lessgtr$ and the G^r (retarded) and G^a (advanced), which are defined as

$$G^r(1,2) = \theta(t_1 - t_2)[G^>(1,2) - G^<(1,2)] \tag{6}$$

$$G^a(1,2) = \theta(t_2 - t_1)[G^<(1,2) - G^>(1,2)] \tag{7}$$

$G^{r,a}$ deal with the dynamics of carriers and $G^\lessgtr$ with the statistics. The Dyson equations for $G^\lessgtr$ and $G^{r,a}$ are obtained from the Dyson equation for the contour ordered Green's function (2) by applying the rules of Langreth.[56]

Under steady state condition the Green's functions depend only on time differences. One usually Fourier transforms the time difference coordinate, $\tau = t - t'$, to energy. Any Green's function G transformed as $G(\mathbf{r}_1, \mathbf{r}_2; E) = \int d\tau e^{iE\tau/\hbar} G(\mathbf{r}_1, \mathbf{r}_2; \tau)$. Under steady-state condition the Dyson equation for the Green's functions can be written as:[57]

$$(E - H_0(\mathbf{r}_1))G^{r,a}(\mathbf{r}_1, \mathbf{r}_2; E) - \int d\mathbf{r}_3 \Sigma^{r,a}(\mathbf{r}_1, \mathbf{r}_3; E) G^{r,a}(\mathbf{r}_3, \mathbf{r}_2; E) = \delta(\mathbf{r}_1 - \mathbf{r}_2) \tag{8}$$

RESEARCH ARTICLE

$$G^{\lessgtr}(\mathbf{r}_1, \mathbf{r}_2; E) = \int d\mathbf{r}_3 \int d\mathbf{r}_4 G^{\mathrm{r}}(\mathbf{r}_1, \mathbf{r}_3; E)\Sigma^{\lessgtr}(\mathbf{r}_3, \mathbf{r}_4; E) \times G^{\mathrm{a}}(\mathbf{r}_4, \mathbf{r}_2; E) \tag{9}$$

where H_0 is the single-particle Hamiltonian operator defined in (4).

2.2. Boundary Conditions and Contact Self-Energies

In order to solve the system of equations discussed above in a finite system, boundary conditions have to be specified. The boundary conditions of (8) and (9) have to model the contacts, which act as a source or drain for electrons. Due to the transitions between the device and the lead, this type of boundary condition can be imposed by adding contact self-energies to the total self-energy.[14,23,57] The self-energies due to contacts are only non-zero at the boundaries[57]

$$\Sigma^{\mathrm{r}}_{\mathrm{s,d}}(E) = \tau^2 g_{\mathrm{s,d}} \tag{10}$$

$$\Sigma^{<}_{\mathrm{s,d}}(E) = -2i\Im m[\Sigma^{\mathrm{r}}_{\mathrm{s,d}}] f_{\mathrm{s,d}}(E) \tag{11}$$

$$\Sigma^{>}_{\mathrm{s,d}}(E) = +2i\Im m[\Sigma^{\mathrm{r}}_{\mathrm{s,d}}](1 - f_{\mathrm{s,d}}(E)) \tag{12}$$

where τ is the coupling matrix between the device and the contact, $f_c(E)$ is the Fermi-Dirac distribution function at the contact c, and g_c is the surface Green's function. The calculation of the surface Green's function is described in Refs. [37, 41, 45, 57].

2.3. Scattering Self-Energies

Using a perturbation expansion one can define the self-energy Σ as an irreducible part of the Green's function. An exact evaluation of the self-energy is possible only for some rather pathological models. For real systems one has to rely on approximation schemes. In this work, the lowest-order self-energy for electron–phonon interaction within the self-consistent Born approximation has been applied.[57]

$$\Sigma^{<}_{\text{el-ph}}(\mathbf{r}, \mathbf{r}'; E) = \sum_j \int \frac{d\mathbf{q}}{(2\pi)^3} e^{i\mathbf{q}\cdot(\mathbf{r}-\mathbf{r}')} D_{\mathbf{q},j} \times \left(n(\hbar\omega_{\mathbf{q},j}) + \frac{1}{2} \pm \frac{1}{2}\right) \times G^{<}(\mathbf{r}, \mathbf{r}'; E \pm \hbar\omega_{\mathbf{q},j}) \tag{13}$$

$$\Sigma^{>}_{\text{el-ph}}(\mathbf{r}, \mathbf{r}'; E) = \sum_j \int \frac{d\mathbf{q}}{(2\pi)^3} e^{i\mathbf{q}\cdot(\mathbf{r}-\mathbf{r}')} D_{\mathbf{q},j} \times \left(n(\hbar\omega_{q,j}) + \frac{1}{2} \pm \frac{1}{2}\right) \times G^{>}(\mathbf{r}, \mathbf{r}'; E \mp \hbar\omega_{\mathbf{q},j}) \tag{14}$$

$$\Sigma^{\mathrm{R}}_{\text{el-ph}}(\mathbf{r}, \mathbf{r}'; E) = -\frac{i}{2}\Gamma_{\text{el-ph}}(\mathbf{r}, \mathbf{r}'; E) + \mathrm{P}\int \frac{dE'}{2\pi} \frac{\Gamma_{\text{el-ph}}(\mathbf{r}, \mathbf{r}'; E')}{E - E'} \tag{15}$$

Here, $\hbar\omega_{\mathbf{q},j}$ denotes the phonon energy of branch j at the wave-vector $\mathbf{q}$, $n(\hbar\omega_{\mathbf{q},j})$ is the average phonon occupation number, $D_{\mathbf{q},j}$ is the the electron–phonon interaction strength, $\Gamma_{\text{el-ph}} \equiv i(\Sigma^{>}_{\text{el-ph}} - \Sigma^{<}_{\text{el-ph}})$ defines the broadening, and $\mathrm{P}\int$ represents the principal part of the integration. The imaginary part of the retarded self-energy broadens the density of states, whereas the real part shifts it in energy. The plus and minus signs in (13) and (14) denote the phonon emission and absorption processes, respectively. Assuming that the bath of phonons is maintained in thermal equilibrium, $n(\hbar\omega_{\mathbf{q},j})$ is given by the Bose-Einstein statistics

$$n(\hbar\omega_{\mathbf{q},j}) = \frac{1}{\exp(\hbar\omega_{\mathbf{q},j}/k_{\mathrm{B}}T) - 1} \tag{16}$$

3. IMPLEMENTATION

In Graph three σ bonds hybridize in an sp^2 configuration, whereas the other $2p_z$ orbital, which is perpendicular to the graphite layer, forms π covalent bonds. The π energy bands are predominantly determining the solid state properties of graphite. Similar considerations hold for CNTs. We use a nearest-neighbor tight-binding π-bond model.[37] Each atom of an sp^2-coordinated CNT has three nearest neighbors, located $a_{\mathrm{cc}} = 1.42$ Å away. The band-structure consists of π-orbitals only, with the hopping parameter $t = V_{pp\pi} \approx -2.77$ eV and the on-site potential $\epsilon_{2p} = 0$. The tight-binding Hamiltonian matrix for a $(n, 0)$ zigzag CNT, shown in Figure 2, can be written as

$$\mathbf{H} = \begin{pmatrix} \mathbf{U}_1 & \mathbf{t}_1 & & & & \\ \mathbf{t}_1 & \mathbf{U}_2 & \mathbf{t}_2 & & & \\ & \mathbf{t}_2^{\dagger} & \mathbf{U}_3 & \mathbf{t}_1 & & \\ & & \mathbf{t}_1 & \mathbf{U}_4 & \mathbf{t}_2^{\dagger} & \\ & & & \mathbf{t}_2 & \mathbf{U}_5 & \cdot \\ & & & & \cdot & \cdot \end{pmatrix} \tag{17}$$

where the entries $\mathbf{U}_\mathrm{i}$ and $\mathbf{t}_\mathrm{i}$ denote matrices. Equal electrostatic potential for all carbon atoms within a ring is assumed, therefore $\mathbf{U}_\mathrm{i} = U_i\mathbf{I}$. The first and second kind of interaction matrices between the neighboring rings are denoted by $\mathbf{t}_1$ and $\mathbf{t}_2$. Only the nearest neighbor interaction between carbon atoms is considered. The coupling matrix between layers 1 and 2 (see Fig. 2) is diagonal, $\mathbf{t}_1 = t\mathbf{I}$, where t is the hopping parameter. However, the coupling matrix between layers 2 and 3 is non-diagonal

RESEARCH ARTICLE

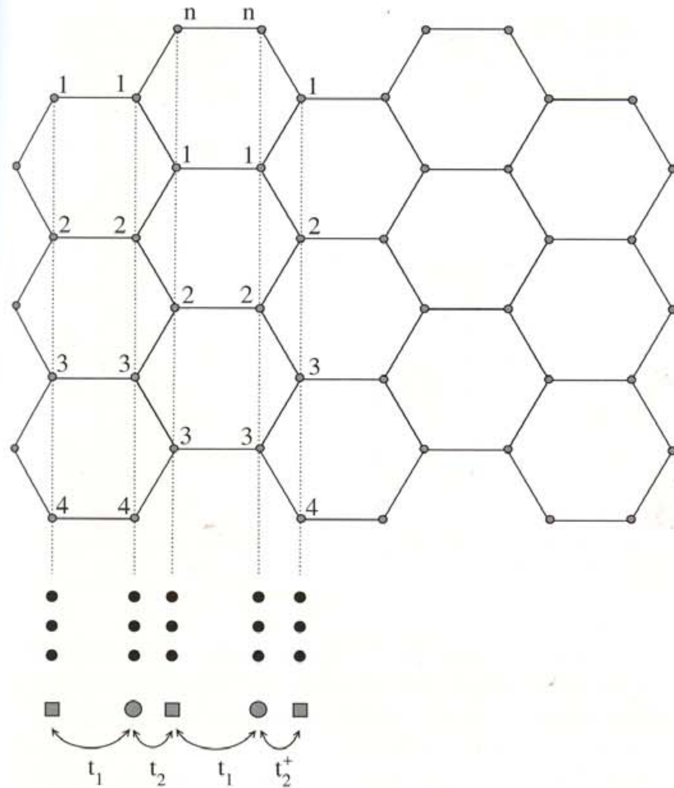

Fig. 2. Layer layout of a $(n, 0)$ zigzag CNT. The coupling matrices between layers are denoted by $\mathbf{t}_1$ and $\mathbf{t}_2$, where $\mathbf{t}_1$ is a diagonal matrix and $\mathbf{t}_2$ includes off-diagonal elements.

$$\mathbf{t}_2 = \begin{pmatrix} t & & & t \\ t & t & & \\ & t & t & \\ & & \cdot & \cdot \end{pmatrix} \tag{18}$$

The eigen-vectors of the matrix $\mathbf{t}_2$ represent plane waves around the circumference of the CNT with the quantized wave-vectors $k_\nu = 2\pi\nu/\sqrt{3}a_{cc}n$, where $\nu = 1, 2, \ldots n$,[37] and the eigen-values $2t\cos(\pi\nu/n)$. By transforming from real space into eigen-mode space,[58] the subbands become decoupled and the Hamiltonian can be written as $\mathbf{H} = \sum_\nu \mathbf{H}^\nu$. The Hamiltonian of the subband ν, $\mathbf{H}^\nu$, is given by

$$\mathbf{H}^\nu = \begin{pmatrix} U_1^\nu & t_1^\nu & & & & \\ t_1^\nu & U_2^\nu & t_2^\nu & & & \\ & t_2^\nu & U_3^\nu & t_1^\nu & & \\ & & t_1^\nu & U_4^\nu & t_2^\nu & \\ & & & t_2^\nu & U_5^\nu & \cdot \\ & & & & \cdot & \cdot \end{pmatrix} \tag{19}$$

where $U_i^\nu = U_i$, $t_1^\nu = t$, and $t_2^\nu = 2t\cos(\pi\nu/n)$.[37,41] The one-dimensional tight-binding Hamiltonian $\mathbf{H}^\nu$ describes a chain with two sites per unit cell with on-site potential U_i^ν and hopping parameters t_1^ν and t_2^ν, see Figure 2. The dispersion relation for each subband ν is given by

$$E^\nu(k_x) = \pm t_0\sqrt{1+2\cos(3a_{cc}k_x/2)\cos(\pi\nu/n)+4\cos^2(\pi\nu/n)} \tag{20}$$

where k_x is the wave-vector along the CNT axis (transport direction). The plus and minus signs in (20) represent the valence and conduction bands, respectively. We consider a (19, 0) zigzag CNT with a band-gap of $E_G = 0.6$ eV. Here devices with zero barrier height for electrons are considered. The one-dimensional equation of motion for the Green's functions have to be solved for $G^{R,\nu}$ and $G^{\lessgtr,\nu}$ for each subband ν. We assume bias conditions for which the first subband contribution need to be considered, therefore the index ν is dropped. To solve (8) and (9) a recursive Green's function algorithm has been used.[23]

Because in CNTs two degrees of freedom are confined, an electron can only be scattered forward or backward in the axial direction, preserving or changing the sign of the band-velocity, respectively. The scattering processes invoke either intra-subband or inter-subband transitions. The intra-subband processes are important for the electrical and the heat transport in CNTs and for the relaxation of an excited electron or hole in the same subband. The inter-subband processes contribute to the radiationless relaxation of electrons (holes) from a given subband to a subband with a lower (higher) energy.[59]

For intra-valley processes, most of the phonons have $\mathbf{q} \approx 0$ and are referred to as Γ-point phonons. Near the Γ point a linear dispersion relation for acoustic phonons is assumed, $\omega_{\mathbf{q},j} \approx v_j|\mathbf{q}|$, where v_j is the acoustic phonon velocity. For optical phonons the energy is assumed to be independent of the phonon wave-vector $\omega_{\mathbf{q},j} \approx \omega_{\mathrm{OP},j} =$ const. Similarly, near the Γ-point the matrix elements of electron–phonon interaction[59] can be approximated as $M_{\mathbf{q},j} \approx M_j^{\mathrm{AP}}|\mathbf{q}|$ for acoustic phonons and $M_{\mathbf{q},j} \approx M_j^{\mathrm{OP}} =$ const for optical phonons. Γ-point phonons belong to the twisting acoustic (TW), the longitudinal the acoustic (LA), the radial breathing mode (RBM), the out-of-phase out-of-plane optical branch (ZO), the transverse optical (TO), or the longitudinal optical (LO) phonon branch. Phonons inducing inter-valley processes have a wave-vector of $|\mathbf{q}| \approx q_K$, where q_K corresponds to the wave-vector of the K-point of the Brillouin zone of graphite. These K-point phonons belong to the E_2', A_2', E_1', or the A_1' phonon branch.[2] K-point phonons, also referred to as zone boundary phonons, are a mixture of fundamental polarizations.

The interaction of electrons with optical phonons is inelastic inelastic. Assuming that the electron–phonon interaction occurs locally,[15] $\Sigma(\mathbf{r}, \mathbf{r}'; E) = 0$ for $\mathbf{r} \neq \mathbf{r}'$, the self-energies can be written as

$$\Sigma_{\mathrm{inel}}^{<}(E) = \sum_j D_{\mathrm{inel},j}\left(n_B(\hbar\omega_j) + \frac{1}{2} \pm \frac{1}{2}\right) G^<(E \pm \hbar\omega_j) \tag{21}$$

RESEARCH ARTICLE

$$\Sigma^{>}_{\text{inel}}(E) = \sum_j D_{\text{inel},j}\left(n_B(\hbar\omega_j) + \frac{1}{2} \pm \frac{1}{2}\right) G^{>}(E \mp \hbar\omega_j) \tag{22}$$

The electron–phonon interaction strength is given by

$$D_{\text{inel},j} = \frac{\hbar |M_j^{\text{OP}}|^2}{2nm_c\omega_j} \tag{23}$$

where m_c is the mass of a carbon atom. Interaction with acoustic phonons can be approximated as elastic scattering, $E \pm \hbar\omega_j \approx E$, and the $n_B(\hbar\omega_j) \approx n_B(\hbar\omega_j) + 1 \approx k_B T/\hbar v_j q$ can be used. Based on this approximation, the self-energies for acoustic phonon interaction simplify to

$$\Sigma^{\lessgtr}_{\text{el}}(E) = D_{\text{el}} G^{\lessgtr}(E) \tag{24}$$

$$D_{\text{el},j} = \frac{k_B T |M_j^{\text{AP}}|^2}{nm_c v_j} \tag{25}$$

The self-energy due to electron–phonon interaction comprises the contributions of elastic and inelastic scattering mechanisms, $\Sigma_{\text{e-ph}} = \Sigma_{\text{el}} + \Sigma_{\text{inel}}$. The transport equations are iterated to achieve convergence of the electron–phonon self-energies, resulting in a self-consistent Born approximation.

To solve the transport equations numerically they need to be discretized in both the spatial and the energy domain. The spatial grid corresponds to the circumferential rings of carbon atoms and is assumed to be uniform. The carrier concentration at some node l of the spatial grid and the current density at the edge between the nodes l and $l+1$ are given by

$$n_l = -4i \int \frac{dE}{2\pi} G^{<}_{l,l}(E) \tag{26}$$

$$j_{l,l+1} = \frac{4q}{\hbar} \int \frac{dE}{2\pi} 2\Re e\{G^{<}_{l,l+1}(E) t_{l+1,l}\} \tag{27}$$

where the factor 4 is due to the spin and band degeneracy. In the Poisson equation, carriers are treated as a sheet charge distributed uniformly over the surface of the CNT.[60] The coupled system of the transport and Poisson equations has to be solved self-consistently.[50] The convergence of the self-consistent iteration is a critical issue. To achieve convergence, fine resonances in $G^{<}(E)$ at some energies have to be resolved accurately.[60,61] For that purpose an adaptive method for selecting the energy grid is essential.[61]

4. THE EFFECT OF SCATTERING PARAMETERS

The electron–phonon coupling strength and the phonon energy depend on the chirality and the diameter of the CNT. The calculation of these parameters is presented in Refs. [59, 62]. In this section the device response is studied for a wide range of electron–phonon interaction parameters.

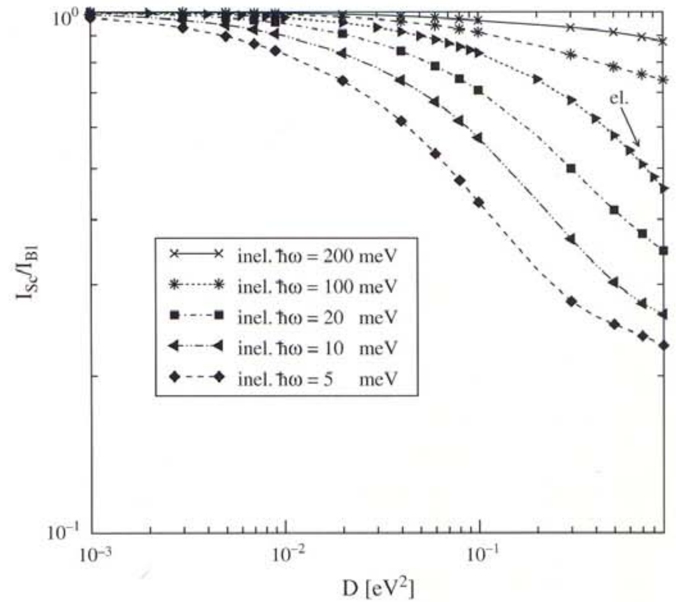

Fig. 3. Ballisticity versus electron–phonon coupling strength for a CNT of 50 nm length. Results for both elastic and inelastic scattering with different phonon energies are shown. $V_G = V_D = 1$ V.

Figure 3 shows the ballisticity as a function of the electron–phonon coupling strength. The ballisticity is defined as I_{Sc}/I_{Bl}, the ratio of the on-current in the presence of electron–phonon interaction to the current in the ballistic case.[63] Elastic scattering conserves the energy of carriers, but the current decreases due to elastic back-scattering. Figure 4 shows that for elastic scattering the source and drain current spectra are symmetric. As the electron–phonon coupling strength increases, resonances

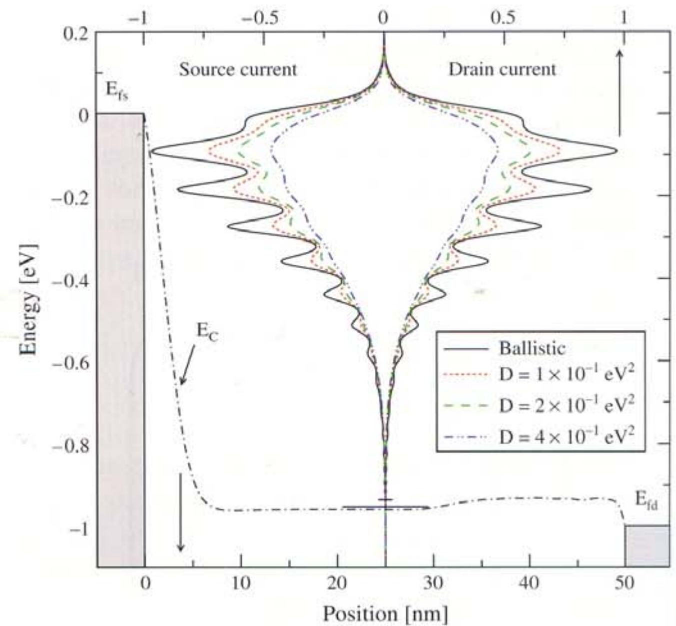

Fig. 4. The spectra of the source and drain currents. The effect of elastic phonon scattering with different coupling strengths is shown. As the coupling strength increases resonances in the current spectrum wash out and the total current reduces due to elastic back-scattering.

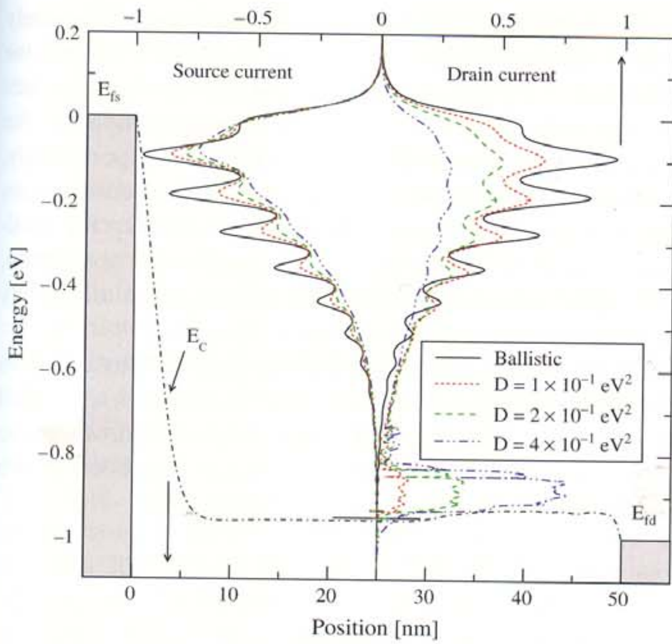

Fig. 5. The spectra of the source and drain currents. The effect of inelastic phonon scattering with different coupling strengths is shown. The phonon energy is $\hbar\omega = 100$ meV. Carriers acquiring enough kinetic energy can emit phonons and scatter into lower energy states. Since the energy of electrons is not conserved in this process, the source and drain current spectrum are not symmetric. As the coupling strength increases more electrons are scattered into lower energy states.

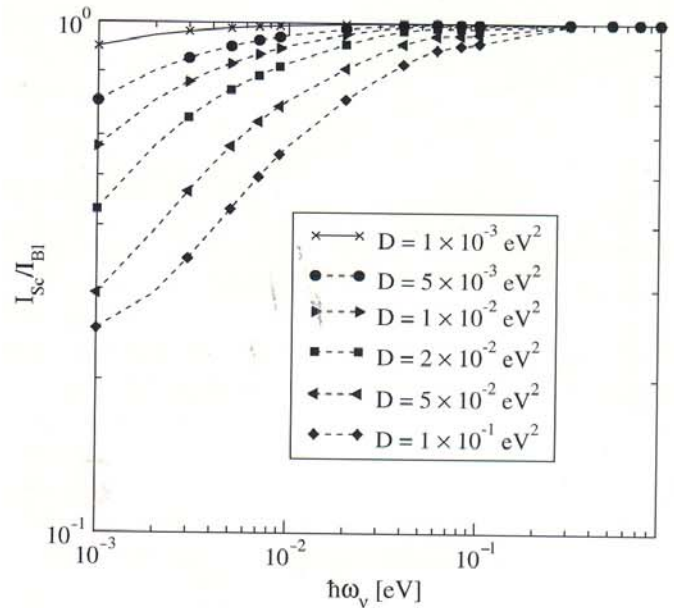

Fig. 7. Ballisticity versus phonon energy for a CNT of 50 nm length. Results for inelastic scattering with different electron–phonon couplings are shown. $V_G = V_D = 1$ V.

in the current spectrum are washed out and the total current reduces due to elastic back-scattering. In the case of inelastic scattering, carriers acquiring enough kinetic energy can emit a phonon and scatter into lower energy states. Therefore, as shown in Figure 5, the source and drain current spectra are not symmetric.

The left part of Figure 6 illustrates an electron losing its kinetic energy by emitting a phonon. The electron will be scattered either forward or backward. In the case of backward scattering the electron faces a thick barrier near the source contact and will be reflected with high probability, such that its momentum will again be directed towards the drain contact.

Figure 7 shows the dependence of the ballisticity with respect to the phonon energy. With increasing phonon energy the effect of phonon scattering on the current is reduced, because scattered electrons lose more kinetic energy and the probability for traveling back to the source

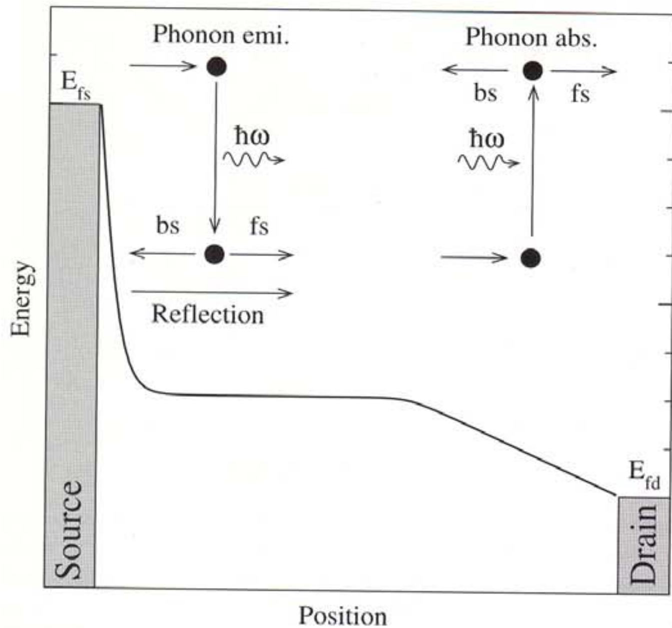

Fig. 6. Sketch of phonon emission and absorption processes in the channel.

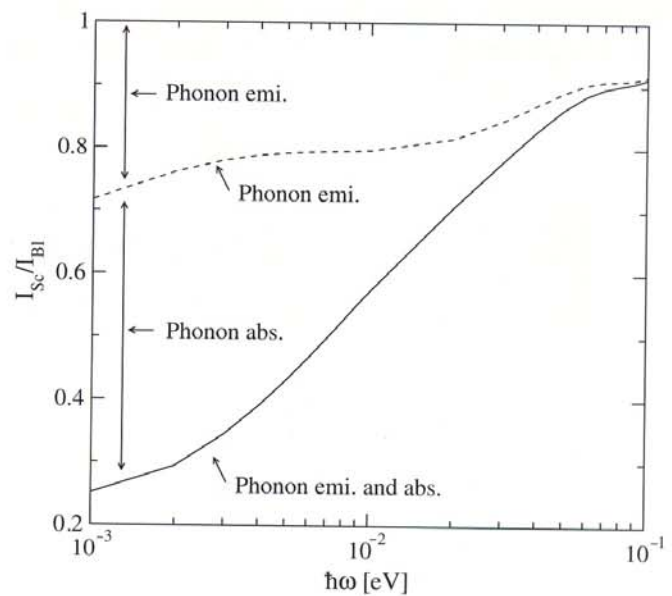

Fig. 8. Ballisticity versus phonon energy with $D_{el} = 10^{-1}$ eV^2 at the bias point $V_G = V_D = 1$ V. The contributions due to phonon absorption and emission are shown.

RESEARCH ARTICLE

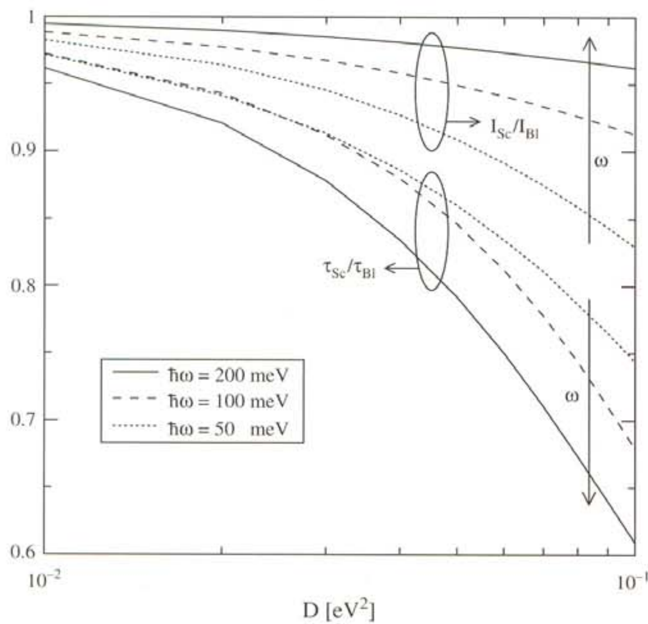

Fig. 9. The ratio of the device delay time in the presence of electron–phonon interaction to the device delay time in the ballistic case, τ_{Sc}/τ_{Bl}, as a function of the electron–phonon coupling strength. For comparison, the I_{Sc}/I_{Bl} is also shown. As the phonon energy increases the device delay time increases. This behavior is due to the reduction of the electron velocity in the channel and the resulting charge pile up.

contact decreases. The considerable decrease of ballisticity for low energy phonons is due to the phonon absorption process. The right part of Figure 6 shows an electron absorbing energy from a phonon and scattering into a higher energy state. In this case, the probability for arriving at the source contact increases. This process can severely reduce the total current. Figure 8 separately shows the effects of the phonon emission and absorption processes on the ballisticity. As the phonon energy reduces, the phonon occupation number (16) increases exponentially, and the self-energy contributions of these two components increase. However, due to the higher probability for back-scattering of electrons in the case of phonon absorption, this component reduces the total current more effectively than the phonon emission process does.

To illustrate the effect of electron–phonon interaction on the dynamic response of the device, the delay time defined as $\tau = (Q_{on} - Q_{off})/I_{on}$ (Ref. [64]) is considered, where the quasi-static approximation is assumed. It has been shown

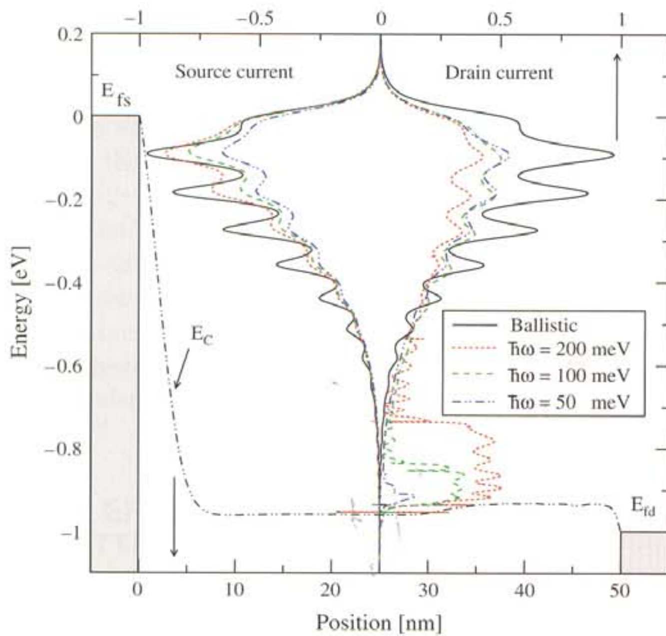

Fig. 10. The spectra of the source and drain currents. The effect of inelastic scattering with different phonon energies is shown. The electron–phonon coupling strength is $D = 2 \times 10^{-1}$ eV². The figure shows a considerable increase of the electron population close to the conduction band-edge as the phonon energy increases.

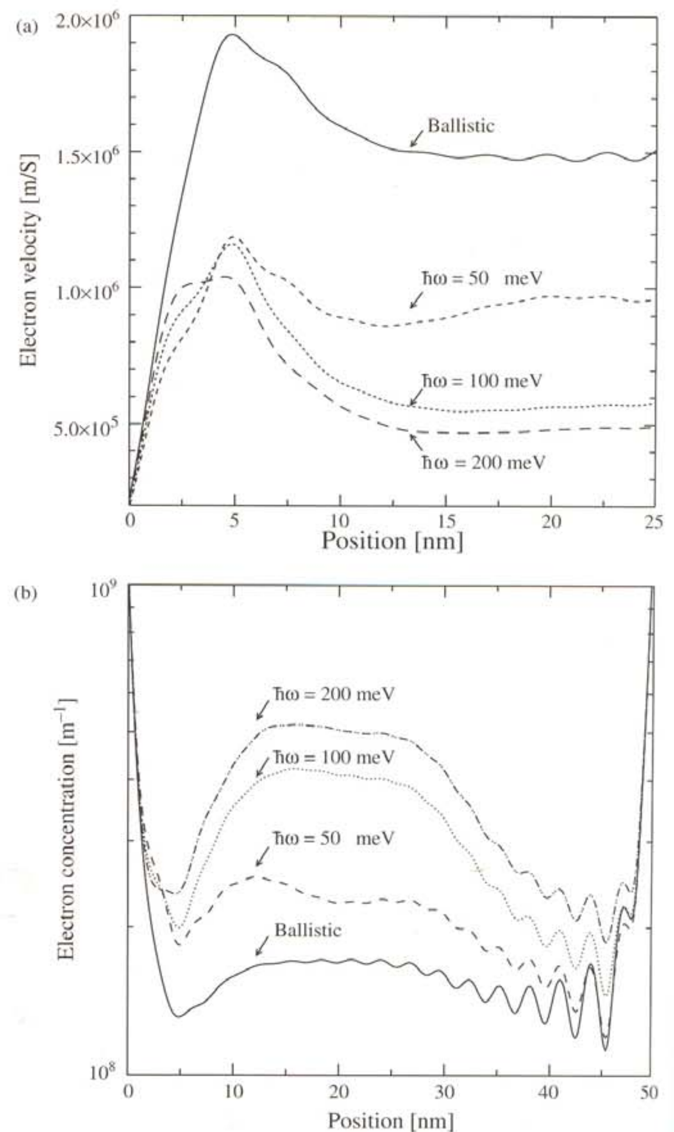

Fig. 11. (a) The profile of the electron velocity near the source contact. (b) The profile of the electron concentration along the device. The results for the ballistic case and for electron–phonon interaction are shown. As the phonon energy increases the electrons scatter to lower energy states, electron decreases more. Therefore, the electron velocity decreases and the carrier concentration increases. The electron–phonon coupling strength is $D = 10^{-1}$ eV² and the bias point is $V_G = V_D = 1$ V.

RESEARCH ARTICLE

that quasi static approximation for CNT based transistors is justified for frequencies below THz.[65] Figure 9 shows the ratio of the device delay time in the presence of electron–phonon interaction to that in the ballistic case, τ_{Sc}/τ_{Bl}, as a function of the electron–phonon coupling strength. As the phonon energy increases the device delay time increases. This behavior can be attributed to the electron group velocity in the channel, which is high for ballistic electrons and low for electrons scattered to lower energy states. Figure 10 shows the spectra of the source and drain currents for different inelastic phonon energies. Electrons can emit a single phonon or a couple of phonons to reach lower energy states. The probability of n sequential electron–phonon interaction decreases as n increases. Therefore, as the phonon energy increases, the occupation of electrons at lower energy states increases. Figure 10 shows a considerable increase of the electron population close to the conduction band-edge as the phonon energy increases. Therefore, as the phonon energy increases the mean velocity of electrons decreases and the carrier concentration in the channel increases (Fig. 11). The increased charge in the channel results in an increased device delay time.

All the above discussed results were calculated for a device with a CNT length of 50 nm. In case of ballistic transport the current is independent of the device length, but in the presence of scattering it reduces as the device length increases. Figure 12 shows the ballisticity as a function of the CNT length in the presence of elastic and inelastic electron–phonon interaction. An artificially large value for the electron–phonon coupling strength and a small value for the phonon energy is chosen to simulate the diffusive limit. In this case, the current is expected to be inversely proportional to the device length according to Ohm's law.

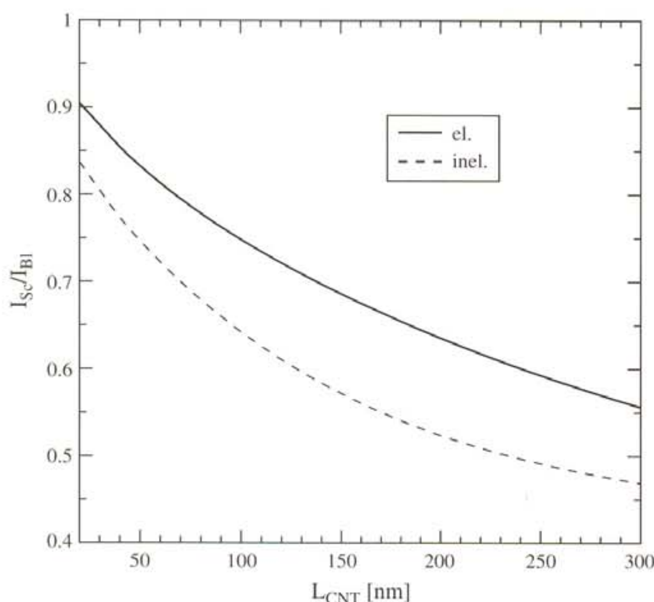

Fig. 12. Ballisticity versus CNT length. The electron–phonon coupling strength for both elastic and inelastic scattering is $D = 10^{-1}$ eV^2, and $\hbar\omega = 25$ meV for inelastic scattering. These scattering parameters simulated the diffusive regime. In this case the ballisticity is inversely proportional to the device length.

5. DISCUSSION

In general the electron–phonon interaction parameters depend on the diameter and the chirality of the CNT. The calculation of these parameters is presented in Refs. [59, 62]. The band gap of a semiconducting CNT is inversely proportional to the diameter. A rough estimate is $E_G = 0.8$ eV/d_{CNT} nm. CNTs with a diameter $d_{CNT} >$ 2 nm have a band gap $E_G < 0.4$ eV, which render them unsuitable as channel for transistors. Since the fabrication of devices with a diameter $d_{CNT} < 1$ nm is very difficult, we limit our study to zigzag CNTs with diameters in the range $d_{CNT} = 1$–2 nm.

Acoustic phonons scattering is treated as an elastic process. Inelastic scattering is induced by OP, RBM, and K-point phonons. Considering the class of CNTs discussed above, the energies of the these phonons are $\hbar\omega_{OP} \approx 200$ meV, $\hbar\omega_{RBM} \approx 30$ meV, and $\hbar\omega_K \approx 160$ and 180 meV.[63, 66] The corresponding coupling coefficients are $D^{OP}_{inel} \approx 40 \times 10^{-3}$ eV^2, $D^{RBM}_{inel} \approx 10^{-3}$ eV^2, and $D^{K}_{inel} \approx 10^{-4}$ and 50×10^{-3} eV^2.[62, 63]

As discussed in Section 4, high energy phonons, such as OP and K-point phonons, reduce the on-current only weakly, but the device delay time can increase considerably due to charge pileup in the channel. Low energy phonons, such as the RBM phonon, can reduce the on-current more effectively, but have a weaker effect on the device delay time. However, due to weak coupling, the RBM mode has a negligible effect at room temperature. The electron–phonon coupling is also weak for acoustic phonon modes ($D^{AP}_{el} < 10^{-3}$ eV^2), which implies that elastic back-scattering of carriers is weak. Therefore, the on-current of short CNT based transistors can be close to the ballistic limit,[1] whereas the switching response can be significantly below that limit.[64, 67–69]

6. CONCLUSIONS

The effect of the electron–phonon interaction parameters on the performance of CNT based transistors was studied numerically, using the NEGF formalism. Elastic scattering is characterized by the electron–phonon coupling strength. For inelastic scattering not only the coupling strength, but also the phonon energy is an important parameter. We showed that elastic back-scattering can reduce the on-current considerably, but the strength of this process is weak in CNTs. Inelastic scattering with high energy phonons reduces the on-current only weakly, whereas it can increase the device delay time considerably. On the other hand, inelastic scattering with low energy phonons

RESEARCH ARTICLE

reduces the on-current considerably, but the effect on the device delay is weak.

Acknowledgment: This work, as part of the European Science Foundation EUROCORES Programme FoNE, was supported by funds from FWF, CNR, EPSRC and the EC Sixth Framework Programme, under Contract N. ERAS-CT-2003-980409.

References

1. A. Javey, J. Guo, D. Farmer, Q. Wang, E. Yenilmez, R. Gordon, M. Lundstrom, and H. Dai, *Nano Lett.* 4, 1319 (**2004**).
2. R. Saito, G. Dresselhaus, and M. Dresselhaus, Physical Properties of Carbon Nanotubes, Imperial College Press, London (**1998**).
3. R. Martel, T. Schmidt, H. Shea, T. Hertel, and P. Avouris, *Appl. Phys. Lett.* 73, 2447 (**1998**).
4. W. Hoenlein, F. Kreupl, G. Duesberg, A. Graham, M. Liebau, R. Seidel, and E. Unger, *IEEE Trans. Components and Packaging Technologies* 27, 629 (**2004**).
5. J. Appenzeller, M. Radosavljevic, J. Knoch, and P. Avouris, *Phys. Rev. Lett.* 92, 048301 (**2004**).
6. A. Javey, J. Guo, Q. Wang, M. Lundstrom, and H. Dai, *Nature (London)* 424, 654 (**2003**).
7. C. Caroli, R. Combescot, P. Nozieres, and D. Saint-James, *J. Phys. C: Solid State Phys.* 4, 916 (**1971**).
8. C. Caroli, R. Combescot, D. Lederer, P. Nozieres, and D. Saint-James, *J. Phys. C: Solid State Phys.* 4, 2598 (**1971**).
9. R. Combescot, *J. Phys. C: Solid State Phys.* 4, 2611 (**1971**).
10. C. Caroli, R. Combescot, P. Nozieres, and D. Saint-James, *J. Phys. C: Solid State Phys.* 5, 21 (**1972**).
11. G. Kim and G. B. Arnold, *Phys. Rev. B* 38, 3252 (**1988**).
12. E. V. Anda and F. Flores, *J. Phys.: Condensed Matter* 3, 9087 (**1991**).
13. L. Y. Chen and C. S. Ting, *Phys. Rev. B* 43, 4534 (**1991**).
14. R. Lake, G. Klimeck, R. C. Bowen, and D. Jovanovic, *J. Appl. Phys.* 81, 7845 (**1997**).
15. R. Lake and S. Datta, *Phys. Rev. B* 45, 6670 (**1992**).
16. C. H. Grein, E. Runge, and H. Ehrenreich, *Phys. Rev. B* 47, 12590 (**1993**).
17. G. Kim, H. Suh, and E. Lee, *Phys. Rev. B* 52, 2632 (**1995**).
18. G. Klimeck, R. Lake, R. C. Bowen, and W. R. Frensley, *Appl. Phys. Lett.* 67, 2539 (**1995**).
19. R. C. Bowen, G. Klimeck, R. K. Lake, W. R. Frensley, and T. Moise, *J. Appl. Phys.* 81, 3207 (**1997**).
20. M. J. McLennan, Y. Lee, and S. Datta, *Phys. Rev. B* 43, 13846 (**1991**).
21. C. Rivas, R. Lake, G. Klimeck, W. R. Frensley, M. V. Fischetti, P. E. Thompson, S. L. Rommel, and P. R. Berger, *Appl. Phys. Lett.* 78, 814 (**2001**).
22. C. Rivas, R. Lake, W. R. Frensley, G. Klimeck, P. E. Thompson, S. L. Rommel, and P. R. Berger, *J. Appl. Phys.* 94, 5005 (**2003**).
23. A. Svizhenko, M. P. Anantram, T. R. Govindan, B. Biegel, and R. Venugopal, *J. Appl. Phys.* 91, 2343 (**2002**).
24. A. Svizhenko and M. P. Anantram, *IEEE Trans. Electron Devices* 50, 1459 (**2003**).
25. R. Venugopal, M. Paulsson, S. Goasguen, S. Datta, and M. S. Lundstrom, *J. Appl. Phys.* 93, 5613 (**2003**).
26. M. B. Nardelli, *Phys. Rev. B* 60, 7828 (**1999**).
27. J. Taylor, H. Guo, and J. Wang, *Phys. Rev. B* 63, 245407 (**2001**).
28. H. Mehrez, J. Taylor, H. Guo, J. Wang, and C. Roland, *Phys. Rev. Lett.* 84, 2682 (**2000**).
29. D. Orlikowski, H. Mehrez, J. Taylor, H. Guo, J. Wang, and C. Roland, *Phys. Rev. B* 63, 155412 (**2001**).
30. M. P. Anantram, *Appl. Phys. Lett.* 78, 2055 (**2001**).
31. A. Maiti, A. Svizhenko, and M. P. Anantram, *Phys. Rev. Lett.* 88, 126805 (**2002**).
32. C.-C. Kaun, B. Larade, H. Mehrez, J. Taylor, and H. Guo, *Phys. Rev. B* 65, 205416 (**2002**).
33. G. Cuniberti, R. Gutiérrez, G. Fagas, F. Grossmann, K. Richter, and R. Schmidt, *Physica E* 12, 749 (**2002**).
34. J. J. Palacios, A. J. P. Jimenez, E. Louis, E. SanFabioa, and J. Verges, *Phys. Rev. Lett.* 90, 106801 (**2003**).
35. Y. Xue and M. A. Ratner, *Appl. Phys. Lett.* 83, 2429 (**2003**).
36. T.-S. Xia, L. F. Register, and S. K. Banerjee, *J. Appl. Phys.* 95, 1597 (**2004**).
37. J. Guo, S. Datta, M. Lundstrom, and M. Anantram, *The International Journal of Multiscale Computational Engineering* 2, 257 (**2004**).
38. J. Guo, *J. Appl. Phys.* 98, 063519 (**2005**).
39. J. Guo, S. Hassan, A. Javey, G. Bosman, and M. Lundstrom, *IEEE Trans. Nanotechnology* 4, 715 (**2005**).
40. A. Svizhenko, M. Anantram, and T. Govindan, *IEEE Trans. Nanotechnology* 4, 557 (**2005**).
41. A. Svizhenko and M. Anantram, *Phys. Rev. B* 72, 085430 (**2005**).
42. M. Brandbyge, J.-L. Mozos, P. Ordejón, J. Taylor, and K. Stokbro, *Phys. Rev. B* 65, 165401 (**2002**).
43. E. Louis, J. A. Vergés, J. J. Palacios, A. J. Pérez-Jiménez, and E. SanFabián, *Phys. Rev. B* 67, 155321 (**2003**).
44. W. Tian, S. Datta, S. Hong, R. Reifenberger, J. I. Henderson, and C. P. Kubiak, *J. Chem. Phys.* 109, 2874 (**1998**).
45. P. S. Damle, A. W. Ghosh, and S. Datta, *Phys. Rev. B* 64, 201403 (**2001**).
46. J. M. Seminario, L. E. Cordova, and P. A. Derosa, *Proc. IEEE* 91, 1958 (**2003**).
47. M. Galperin, A. Nitzan, S. Sek, and M. Majda, *J. Electroanalytical Chem.* 550–551, 337 (**2003**).
48. P. A. Derosa, S. Guda, and J. M. Seminario, *J. Am. Chem. Soc.* 125, 14240 (**2003**).
49. Y. Xue and M. A. Ratner, *Phys. Rev. B* 69, 085403 (**2004**).
50. A. W. Ghosh, T. Rakshit, and S. Datta, *Nano Lett.* 4, 565 (**2004**).
51. J. Schwinger, *J. Math. Phys.* 2, 407 (**1961**).
52. L. P. Kadanoff and G. Baym, Quantum Statistical Mechanics: Green's Function Methods in Equilibrium and Non-Equilibrium Problems, W.A. Benjamin, New York (**1962**).
53. P. Danielewicz, *Ann. Phys.* 152, 239 (**1984**).
54. W. Schäfer and M. Wegener, Semiconductor Optics and Transport Phenomena, Springer, Berlin, New York (**2002**).
55. L. V. Keldysh, *Soviet Phys. JETP*, 20, 1018 (**1965**).
56. D. C. Langreth, Linear and non-linear electron transport in solids, ser. NATO Advanced Study Institute Series: Series B, Plenum Press, New York (**1976**), Vol. 17, pp. 3–18.
57. S. Datta, Electronic Transport in Mesoscopic Systems, Cambridge University Press, New York (**1995**).
58. R. Venugopal, Z. Ren, S. Datta, M. Lundstrom, and D. Jovanovic, *J. Appl. Phys.* 92, 3730 (**2002**).
59. V. N. Popov and P. Lambin, *Phys. Rev. B* 74, 075415 (**2006**).
60. D. John, L. Castro, P. Pereira, and D. Pulfrey, *Proc. NSTI Nanotech.* (**2004**), Vol. 3, pp. 65–68.
61. M. Pourfath and H. Kosina, Fast Convergent Schrödinger-Poisson Solver for the Static and Dynamic Analysis of Carbon Nanotube Field Effect Transistors. Lecture Notes in Computer Science, Springer Berlin/Heidelberg (**2006**), Vol. 3743, pp. 578–585.
62. G. D. Mahan, *Phys. Rev. B* 68, 125409 (**2003**).
63. S. O. Koswatta, S. Hasan, M. Lundstrom, M. P. Anantram, and D. E. Nikonov, *Appl. Phys. Lett.* 89, 023125 (**2006**).

64. Y. Yoon, Y. Ouyang, and J. Guo, *IEEE Trans. Electron Devices* 53, 2467 (**2006**).

65. Y. Chen, Y. Ouyang, J. Guo, and T. X. Wu, *Appl. Phys. Lett.* 89, 203122 (**2006**).

66. J. Park, S. Rosenblatt, Y. Yaish, V. Sazonova, H. Ustunel, S. Braig, T. Arias, P. Brouwer, and P. McEuen, *Nano Lett.* 4, 517 (**2004**).

67. D. Singh, K. Jenkins, J. Appenzeller, D. Neumayer, A. Grill, and H.-S. P. Wong, *IEEE Trans. Nanotechnology* 3, 383 (**2004**).

68. D. Frank and J. Appenzeller, *IEEE Trans. Electron Devices* 25, 34 (**2004**).

69. L. Castro, D. John, D. Pulfrey, M. Pourfath, A. Gehring, and H. Kosina, *IEEE Trans. Nanotechnology* 4, 699 (**2005**).

Received: 21 March 2007. Accepted: 4 May 2007.